PRAMANA
— journal of
physics

Vol. 63, No. 3
September 2004
pp. 563–577

Electron cyclotron resonance heating in a short cylindrical plasma system

VIPIN K YADAV and D BORA
Institute for Plasma Research, Bhat, Gandhinagar 382 428, India
E-mail: vipin@ipr.res.in; dbora@ipr.res.in

MS received 22 April 2003; revised 29 March 2004; accepted 5 May 2004

Abstract. Electron cyclotron resonance (ECR) plasma is produced and studied in a small cylindrical system. Microwave power is delivered by a CW magnetron at 2.45 GHz in TE_{10} mode and launched radially to have extraordinary (X) wave in plasma. The axial magnetic field required for ECR in the system is such that the first two ECR surfaces (B = 875.0 G and B = 437.5 G) reside in the system. ECR plasma is produced with hydrogen with typical plasma density n_e as 3.2×10^{10} cm^{-3} and plasma temperature T_e between 9 and 15 eV. Various cut-off and resonance positions are identified in the plasma system. ECR heating (ECRH) of the plasma is observed experimentally. This heating is because of the mode conversion of X-wave to electron Bernstein wave (EBW) at the upper hybrid resonance (UHR) layer. The power mode conversion efficiency is estimated to be 0.85 for this system. The experimental results are presented in this paper.

Keywords. X-wave; electron cyclotron resonance; upper hybrid resonance.

PACS Nos 52.35.Hr, 52.50.Sw, 52.70.Gw

1. Introduction

The interaction of electromagnetic (EM) wave with the plasma is studied for the last few decades. These studies also include ECR-produced plasmas for its broad range of applications including plasma production [1] and plasma heating [2]. This plasma heating by EM waves (in microwave range) is done in fusion machines such as tokamaks [3] and stellarators [4] or in mirror machines [5]. The ECR condition has also found application in electron cyclotron current drive (ECCD) in fusion machines by ECR-induced transport [6].

Although ECRH, as an auxiliary heating scheme is used in the fusion experiments all over the world, many basic phenomena and physical processes in ECR-produced plasmas are still not well-investigated. To study these ECR-produced plasmas and related physical processess, experimental set-ups in the form of small toroidal systems are designed to carry out basic experiments [1,7,8]. As the effect of system geometry is generally not of much significance in ECR because of higher frequencies

(few GHz) of microwave sources, a small linear ECR plasma system can also serve the purpose [9–11]. Localized shell-like hot electron layers in ECR-driven plasmas are studied in small linear systems [12]. High pressure, partially ionized plasma is produced using ECR for surface treatment [13]. ECR plasma can also be studied with better magnetic confinement in linear mirror machines using standard 2.45 GHz frequency source [14].

In this paper we report the small linear system designed to perform basic experiments. ECR plasma is produced with hydrogen in the plasma system. Various cut-offs and resonances which reside in the system are identified. Plasma heating because of the generation of highly energetic electrons at the two ECR layers is observed experimentally. This plasma heating is verified by various other direct and indirect methods. Ultra-soft x-ray emission is also observed from the ECR-produced plasma which confirms the plasma heating. These experimental observations are discussed in the paper.

The paper is organized as follows: In §2, the theoretical aspects of X-mode propagation and absorption in ECR plasma, to identify various physical processes involved, are discussed. Section 3 is dedicated to the experimental set-up and the main diagnostics. Section 4 contains the presentation and interpretation of the main experimental results. Section 5 contains the discussion and the final conclusion.

2. Theoretical aspects

2.1 *Resonances and cut-offs in X-mode propagation*

In the EM wave propagation in X-mode, the wave electric field $\vec{E}$ is perpendicular to the ambient magnetic field $\vec{B}_0$, ($\vec{E} \perp \vec{B}_0$) as well as the wave vector $\vec{k}$, ($\vec{E} \perp \vec{k}$). The dispersion relation for the X-wave [15,16] is

$$\frac{c^2k^2}{\omega^2} = \frac{c^2}{v_\phi^2} = 1 - \frac{\omega_{\rm pe}^2}{\omega^2}\frac{\omega^2 - \omega_{\rm pe}^2}{\omega^2 - \omega_{\rm uh}^2}. \tag{1}$$

Here c is the velocity of light in vacuum, ω is the launched wave angular frequency and $\omega_{\rm uh}$ is the UHR frequency given by

$$\omega_{\rm uh}^2 = \omega_{\rm pe}^2 + \omega_{\rm ce}^2, \tag{2}$$

where $\omega_{\rm pe} = (n_{\rm e}e^2/m_{\rm e}\epsilon_0)^{1/2}$ is the angular electron plasma frequency and $\omega_{\rm ce} = eB_0/m_{\rm e}$ is the angular electron cyclotron frequency, $n_{\rm e}$ is the electron plasma density, e is the electron charge, $m_{\rm e}$ is the electron mass and ϵ_0 is the permittivity of free space.

The X-wave dispersion [17] as v_ϕ^2/c^2 with ω is shown in figure 1. The wave is propagating from the right to the left side in the figure. The resonance occurs when $\vec{k} \to \infty$. In eq. (1), $\vec{k} \to \infty$ occurs at $\omega = \omega_{\rm uh}$. The UHR layer lies in between the first ECR surface B_1 and the second ECR surface B_2.

The cut-off occurs when $\vec{k} \to 0$. This condition for this X-wave in the plasma is satisfied when in eq. (1)

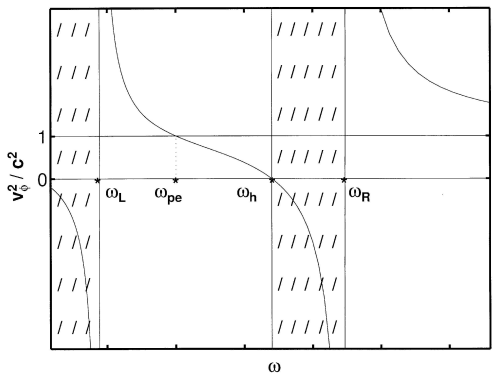

Figure 1. The dispersion curve for X-mode. The wave does not propagate in the shaded region.

$$\frac{\omega_{\rm pe}^2}{\omega^2}\frac{\omega^2-\omega_{\rm pe}^2}{\omega^2-\omega_{\rm uh}^2}=1. \tag{3}$$

The equation is simplified to have

$$\omega^2 \pm \omega\omega_{\rm ce}=\omega_{\rm pe}^2. \tag{4}$$

This equation gives two cut-offs as

$$\begin{aligned}\omega_{\rm L}&=\frac{1}{2}\left(\omega_{\rm ce}+\sqrt{(\omega_{\rm ce}^2+4\omega_{\rm pe}^2)^*}\right),\\ \omega_{\rm R}&=\frac{1}{2}\left(-\omega_{\rm ce}+\sqrt{(\omega_{\rm ce}^2+4\omega_{\rm pe}^2)^*}\right).\end{aligned} \tag{5}$$

Here, $\omega_{\rm L}$ is the left-hand X-mode cut-off on the left side and $\omega_{\rm R}$ is the right-hand X-mode cut-off on the right side of the UHR layer as shown in figure 1.

The incident X-wave will be reflected at the cut-off and give rise to a standing wave in the waveguide as well as a wave-field trapped between the cut-off surface and the outer wall. The launched microwave power will tunnel through the cut-off surface in the form of ordinary O-mode wave which is generated due to the reflection of X-mode from the wall. This O-mode wave is converted back to the X-mode by reflection from the inner wall, and this reflected wave reaches the UHR and gets absorbed there.

2.2 *Absorption of the X-mode in ECR plasma*

The launched X-mode in ECR plasma is absorbed through the mode conversion of EM wave (X-wave) into electrostatic (ES) wave (EBW). This mode conversion from EM wave to EBW (X-B process) takes place for $n_\parallel \approx 0$ with mode conversion efficiency C depending on the electron density scale length ($L_{\rm n}$) in the mode conversion region at UHR layer.

The X-mode tunneling through the evanescent region between the cut-off and the UHR is taken from the cold plasma theory [18,19]. The power mode conversion coefficient C is given as

$$C = C_{\max} \cos^2\left(\frac{\phi}{2} + \theta\right),$$
$$C_{\max} = 4\mathrm{e}^{-\pi\eta}(1 - \mathrm{e}^{-\pi\eta}), \tag{6}$$

where $\cos^2(\phi/2 + \theta)$ is the phase factor of the wave in the mode conversion region, η is the Budden parameter and ϕ is the phase difference between the slow X-mode propagating towards the left cut-off and the reflected component propagating towards the UHR layer. θ is given by

$$\theta = \arg\,\Gamma\left(\frac{-i\eta}{2}\right). \tag{7}$$

The Budden parameter η is given as

$$\eta = \frac{\omega_{\mathrm{ce}} L_{\mathrm{n}}}{c} \frac{\alpha}{\sqrt{\alpha^2 + 2(L_{\mathrm{n}}/L_{\mathrm{B}})}} \left[\frac{\sqrt{1+\alpha^2} - 1}{\alpha^2 + (L_{\mathrm{n}}/L_{\mathrm{B}})\sqrt{1+\alpha^2}}\right]^{1/2},$$
$$\alpha = \left[\frac{\omega_{\mathrm{pe}}}{\omega_{\mathrm{ce}}}\right]_{\mathrm{UHR}} \tag{8}$$

L_{n} is the density scale length and L_{B} is the magnetic field scale length evaluated at the UHR layer. For $L_{\mathrm{B}} \gg L_{\mathrm{n}}$, eq. (8) reduces to

$$\eta \approx \frac{\omega_{\mathrm{ce}} L_{\mathrm{n}}}{\alpha c}[\sqrt{1+\alpha^2} - 1]^{1/2}. \tag{9}$$

In the following experiment, microwaves of angular frequency $\omega = 2\pi f = 1.54 \times 10^{10}$ rad/s are launched into the plasma perpendicular to B_0.

2.3 *Electron energy distribution function (EEDF)*

Langmuir probe diagnostics [20] is a common method for measuring different plasma parameters. As an indirect method, the notion of obtaining EEDF from Langmuir probe characteristics is given by Druyvesteyn [21]. Later on this method was used to measure the EEDF in low pressure RF discharges [22] and for determining EEDF in plasmas excited by ECR [23].

In Langmuir probe characteristics, the probe current, I_{sat} (for $V_{\mathrm{p}} \geq V_{\mathrm{B}}$) is given by [20]

$$I_{\mathrm{sat}} = S n_{\mathrm{e}} e \sqrt{T_{\mathrm{e}}/2\pi m_{\mathrm{e}}} \exp\left[\frac{-e(V_{\mathrm{p}} - V_{\mathrm{B}})}{T_{\mathrm{e}}}\right]. \tag{10}$$

Here V_{B} is the bias voltage on probe, V_{p} is the plasma potential, S is the charge collecting area of the probe, T_{e} is the plasma temperature and m_{e} is the mass of the electron.

Differentiating eq. (10) with respect to V_{B}, we get

$$\frac{\partial I_{\mathrm{sat}}}{\partial V_{\mathrm{B}}} = \frac{e^2 S n_{\mathrm{e}}}{\sqrt{2\pi m_{\mathrm{e}} T_{\mathrm{e}}}} \exp\left[\frac{-e(V_{\mathrm{p}} - V_{\mathrm{B}})}{T_{\mathrm{e}}}\right]. \tag{11}$$

For non-drifting Maxwellian plasmas this derivative is proportional to the electron distribution function f_ϵ which is given as

$$\frac{\partial I_{\mathrm{sat}}}{\partial V_{\mathrm{B}}} = \frac{e f_z(v_z)}{T_{\mathrm{e}}} \propto f(\epsilon). \tag{12}$$

Equation (11) is simplified by defining $f(V)$ as

$$f(V) = \frac{M}{\sqrt{2\pi m_{\mathrm{e}} T_{\mathrm{e}}}} \exp\left[\frac{-e(V_{\mathrm{p}} - V_{\mathrm{B}})}{T_{\mathrm{e}}}\right],$$
$$M = n_{\mathrm{e}} m_{\mathrm{e}}. \tag{13}$$

The EEDF is then given by

$$f(V) = \frac{m_{\mathrm{e}}}{e^2 S} \frac{\mathrm{d}I}{\mathrm{d}V} \tag{14}$$

and V is given by

$$V = V_{\mathrm{p}} - V_{\mathrm{B}}. \tag{15}$$

Here V_{p} is the plasma potential and V_{B} is the bias voltage on the probe.

2.4 *Wave electric field measurements*

2.4.1 *Wave-field of the incident wave*: The electric field E_0 of the incident EM wave in the waveguide [24] is given by

$$E_0 = 2\left[\frac{\omega \mu_0 P}{\beta_g a b}\right]^{1/2}, \tag{16}$$

where a is the broader and b is the shorter dimension of the waveguide, P is the launched power and $\omega = 2\pi f$ is the angular frequency of the incident EM wave. For wave frequency f, β_g is the phase constant given by

$$\beta_g = \pi\sqrt{\left(\frac{2f}{c}\right)^2 - \frac{1}{a^2}}. \tag{17}$$

Here, c is the velocity of light in free space. For WR340 waveguide used in this experiment having $a = 86$ mm, $b = 43$ mm, $f = 2.45 \times 10^9$ Hz, β_g comes out to be 132.7π and eq. (16) then becomes

$$E_0 = 224\sqrt{P}\ V/m. \tag{18}$$

Here P is in Watt.

2.4.2 *Wave-field of the outcoming wave*: As the EM wave launched in the plasma is in X-mode, initially $N_{\parallel} = 0$ but as the wave travels through the plasma it gets mode converted to EBW at UHR and attains a finite $N_{\parallel}$ because of the scattering from the plasma particles or due to magnetic configuration such as the field line curvature. To come out of the plasma, this EBW backconverts to EM wave and comes out at an angle ϕ (viewing angle) [25,26] given by

$$N_{\parallel,\text{opt.}} = \cos^2\phi = Y/(Y+1)$$
$$Y = \omega_{\text{ce}}/\omega. \tag{19}$$

For $f = \omega/2\pi = 2.45$ GHz, $[B_0]_{\text{uhr}} = 769$ G, $Y = 0.88$ and hence $N_{\parallel,\text{opt.}} = 0.47$ which gives a viewing angle of $\phi = 46.84°$.

The waves which will come out because of their $N_{\parallel}$ component will undergo a temporal and spatial resonance which means that the frequency and wavelength of the incident wave will not change after the mode conversion. The power of the incoming wave is expected to be reduced because of the finite plasma conductivity and due to the collisions with the plasma particles.

2.5 *Plasma parameters*

2.5.1 *Estimation of plasma density,* n_{e}: The electron fluid velocity is given by

$$v_{\text{fluid}} = \frac{eE}{m_{\text{e}}\nu}\left(\frac{\nu^2}{\nu^2+\omega^2}\right), \tag{20}$$

where e is the electron charge, E is the wave electric field, ν is the elastic electron-neutral collision frequency, m_{e} is the electron mass and ω is the angular frequency of the launched wave. For $\nu \ll \omega$, the above equation reduces to

$$v_{\text{fluid}} \approx \frac{eE\nu}{m_{\text{e}}\omega^2}. \tag{21}$$

The average oscillating energy ($\mathcal{E}$) of the electron motion in the wave is given by

$$\mathcal{E} = \frac{e\eta}{4\pi^2 m_{\text{e}} c^2} P_{\text{RF}} \approx 2\times 10^{-5}\ P_{\text{RF}}, \tag{22}$$

where e is the electron charge, η the free air impedance is $\approx$377 Ω, P_{RF} is the launched RF or microwave power, m_{e} is the electron mass and c is the velocity of light in free space. For $P_{\text{RF}} = 800$ W,

$$\mathcal{E} = 1.6\times 10^{-2}\ \text{eV}. \tag{23}$$

This is the energy gained in each collision. This energy is less than the ionization energy for the hydrogen E_{i} ($\approx$13.6 eV). The RMS energy, $\mathcal{E}$ is converted into random energy through elastic collisions which finally results in the electron heating. The number of such elastic collisions ($N_{\text{coll.}}$) required to achieve E_{i} is given by

$$N_{\text{coll.}} = 13.6/(1.6\times 10^{-2}) = 850 \approx 1000. \tag{24}$$

According to the electron fluid model, the average energy transferred to the electrons is given as

$$\begin{aligned} &\mathrm{d}\epsilon/\mathrm{d}t = -e\vec{E}\cdot\vec{v}, \\ &\mathrm{d}\epsilon/\mathrm{d}t \approx 2\nu E_{\mathrm{RMS}}, \end{aligned} \tag{25}$$

where $\vec{E}$ is the wave electric field, $\vec{v}$ is the electron thermal velocity and ν is the electron collision frequency. The power transferred from electrons to neutrals through inelastic collisions is given by the equation

$$P \sim n_{\mathrm{e}} V \nu_{\mathrm{in}} E_{\mathrm{i}} \sim n_{\mathrm{e}} V f \nu_{\mathrm{e}} E_{\mathrm{i}}. \tag{26}$$

For

$$\begin{aligned} &\nu_{\mathrm{in}} = n_{\mathrm{n}} \langle \sigma_{\mathrm{in}} v \rangle \\ &\nu_{\mathrm{e}} = n_{\mathrm{n}} \langle \sigma_{\mathrm{e}} v \rangle \\ &f \sim \nu_{\mathrm{in}}/\nu_{\mathrm{e}}. \end{aligned} \tag{27}$$

From the electron balance equation

$$\begin{aligned} &n_{\mathrm{n}} n_{\mathrm{e}} \langle \sigma_{\mathrm{e}} v \rangle = n_{\mathrm{e}}/\tau_{\mathrm{p}}, \\ &\nu_{\mathrm{e}} = 1/\tau_{\mathrm{p}}, \end{aligned} \tag{28}$$

where n_{n} is the neutral density, n_{e} is the electron density, $\langle \sigma_{\mathrm{e}} v \rangle$ is the rate constant of ionization and τ_{p} is the plasma confinement time. From eqs (26) and (28), we have

$$P = n_{\mathrm{e}} V f E_{\mathrm{i}}/\tau_{\mathrm{p}} \Longrightarrow n_{\mathrm{e}} = P\tau_{\mathrm{p}}/V f E_{\mathrm{i}}. \tag{29}$$

In our experimental set-up $P_{\mathrm{coupled}} = 400$ W, $E_{\mathrm{i}} = 13.6$ eV, $f = 10$ (typically), $\tau_{\mathrm{p}} = 2.5$ μs and $V = 1.29 \times 10^{-3}$ m^3. Using these values, the electron plasma density in the system comes out to be

$$n_{\mathrm{e}} = 3.6 \times 10^{10}\ \mathrm{cm}^{-3}. \tag{30}$$

This matches well with the experimentally determined plasma density n_{e} equals to 3.2×10^{10} cm^{-3} in the system.

2.5.2 *Estimation of plasma temperature,* T_{e}: Equation (28) gives

$$n_{\mathrm{n}} \tau_{\mathrm{p}} = 1/\langle \sigma_{\mathrm{e}} v \rangle. \tag{31}$$

For atomic hydrogen

$$\langle \sigma_{\mathrm{e}} v \rangle = \frac{2 \times 10^{-13}}{6 + T_{\mathrm{e}}/E_{\mathrm{i}}} \left(\frac{T_{\mathrm{e}}}{E_{\mathrm{i}}} \right)^{1/2} \exp\left(\frac{-E_{\mathrm{i}}}{T_{\mathrm{e}}} \right). \tag{32}$$

Here T_{e} is the electron plasma temperature. Equations (31) and (32) give

$$n_{\mathrm{n}} \tau_{\mathrm{p}} \sim 10^{13} \left(3 + \frac{T_{\mathrm{e}}}{2E_{\mathrm{i}}} \right) \left(\frac{E_{\mathrm{i}}}{T_{\mathrm{e}}} \right)^{1/2} \exp\left(\frac{E_{\mathrm{i}}}{T_{\mathrm{e}}} \right). \tag{33}$$

For $\tau_{\rm p} = 2.5$ μs and $n_{\rm n} = 3.3 \times 10^{19}$ m^{-3} for an operating pressure of 1×10^{-3} mbar, plasma temperature in the system can be estimated from figure 2 as

$$T_{\rm e} \approx 10 \text{ eV}. \tag{34}$$

The experimentally observed plasma temperature $T_{\rm e}$ is between 9 and 15 eV which is in good agreement with the theoretical estimation.

3. Experimental set-up

The experimental set-up consists of a cylindrical vacuum vessel, pulsed magnetic field coils for axial magnetic field, power supplies, vacuum pumps, microwave source, diagnostic system, etc.

The stainless steel vacuum chamber which is cylindrical with internal radius 64.1 mm and axial length 100 mm is shown in figure 3. It has five radial ports (four circular and one rectangular) and two axial ports equipped with conflat flanges with teflon gaskets. The vacuum vessel is pumped by a diffusion pump backed by rotary pump. A base pressure of 6×10^{-6} mbar is achieved.

The magnetic field is produced by two identical coils rested on the axial ports at the two ends of the vacuum vessel as shown in figure 4. Each magnetic field coil has an electrical resistance of 30 Ω and requires 5.3 A of DC current to produce magnetic field of 875 G at the axis of the vacuum vessel. The magnetic field variation in radial direction is shown in figure 5. The magnetic field contours in the system are shown in figure 6. These contours indicate the magnetic mirror configuration in the system. The magnetic field rise with time is shown in figure 7 which shows a constant magnetic field for more than 1 s.

The microwave system consists of a 870 W (CW), 2.45 GHz magnetron, a high voltage DC power supply to bias the cathode up to -4.1 kV, a three-port circulator with water-cooled dummy load to take away the reflected power, a WR340

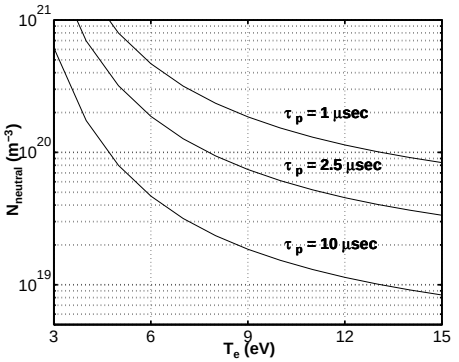

Figure 2. Theoretical estimation of plasma temperature.

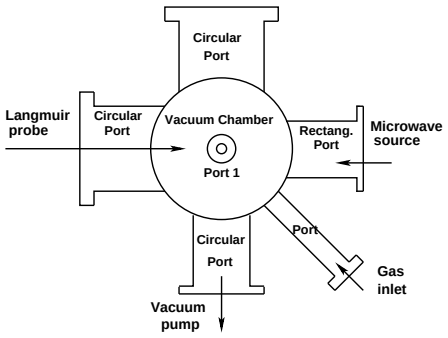

Figure 3. Main chamber (axial view).

directional coupler and low barrier Schottky diode microwave detectors to measure forward and reflected microwave power.

Langmuir or electric probe is the most widely used diagnostics for the characterization of basic plasma parameters in experiments [27]. In our experiments, the plasma is diagnosed by two movable Langmuir probes (probe tip length = 5 mm, probe tip diameter = 0.5 mm) (with Wilson feedthroughs) placed axially and radially to observe the axial and radial variations of plasma parameters. The overall uncertainty in probe-positioning is 1–2 mm.

A movable dipole probe, installed at the top port, is used to measure the wave electric field in plasma. The total length of the dipole probe is 11 mm. The separation between the two receivers of the dipole is 1 mm. The signals from the diagnostic systems are acquired by a four-channel Tektronix TDS 224 model oscilloscope and then transferred to a PC using a RS232 cable and Wavestar software.

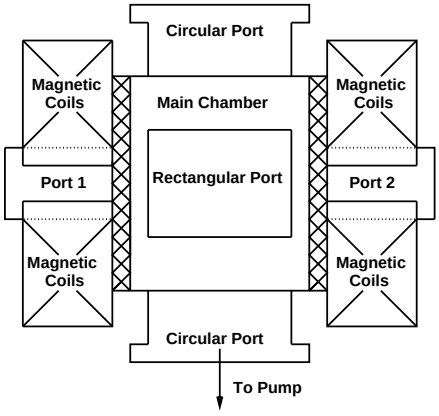

Figure 4. System configuration (radial view).

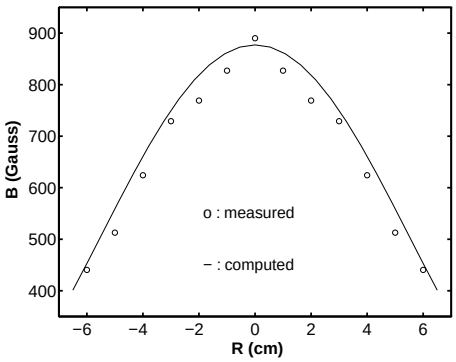

Figure 5. Radial variation of the magnetic field in the system.

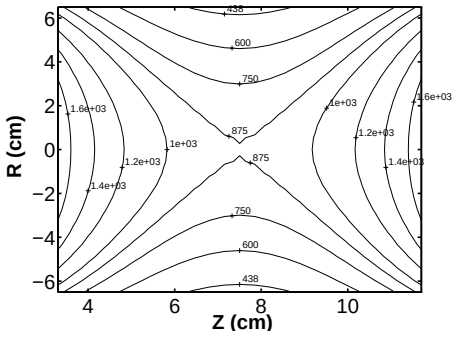

Figure 6. Contour plot of the magnetic field (G) in the system.

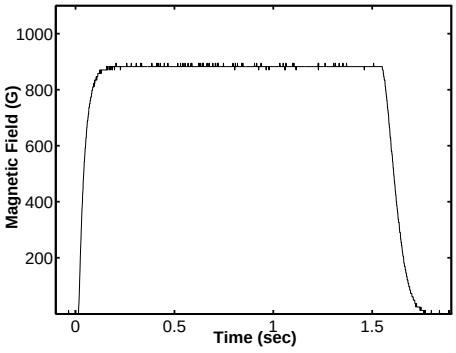

Figure 7. Time evolution of magnetic field.

4. Experimental results

4.1 *Plasma parameters*

(a) *Plasma density* n_e: The axial profile of plasma density at similar experimental conditions as in radial profile, is shown in figure 8. As shown in the figure, the plasma density is constant in the centre and falls down near the walls.

The radial profile of plasma density for hydrogen plasma is measured at an operating pressure of 1×10^{-3} mbar and is shown in figure 9. The typical input power in the chamber is ≈800 W. As evident from the graph, the plasma density n_e in the region $6 > R > 0$ (region near microwave source) is higher compared to the region $-6 < R < 0$, which is on the opposite side of the microwave source. This can be explained in the following manner. The electron cyclotron resonance occurs at the centre and the initial breakdown of the gas takes place here. Plasma starts diffusing in the radial direction across the magnetic field. The fraction of the incident microwave power which is not absorbed in the first pass gets reflected and starts moving backwards toward the source and contribute in further ionization.

(b) *Plasma temperature* T_e: Axial variation of plasma temperature is shown in figure 10. It shows an increase in temperature near the walls. This may be because of the electron trapping at these positions due to the higher values of the magnetic field [28,29].

The magnetic field configuration in this plasma system forms a magnetic mirror with mirror ratio 1.92 as evident from figure 6. The energetic electrons are trapped in this magnetic mirror and retain their energies. Plasma temperature in the radial direction varies between 9 and 15 eV as shown in figure 11.

(c) *Plasma potential* V_p: Typical plasma potential measured in the ECR plasma system is 50 V.

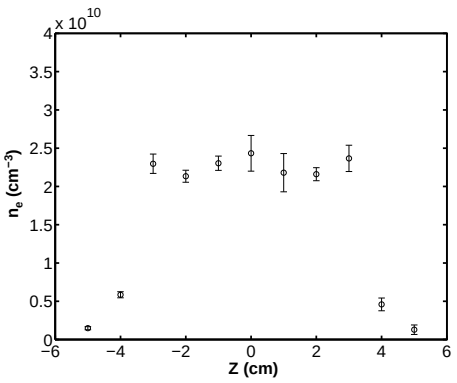

Figure 8. Axial variation of plasma density.

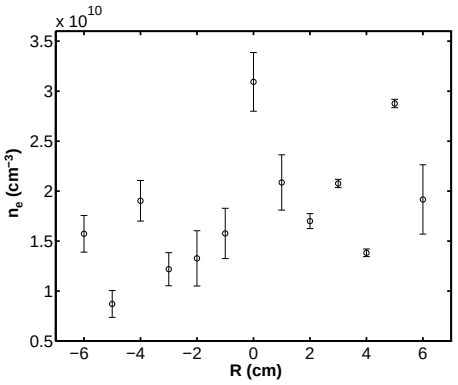

Figure 9. Radial variation of plasma density.

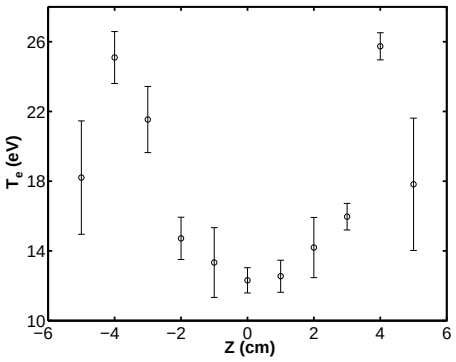

Figure 10. Axial variation of plasma temperature.

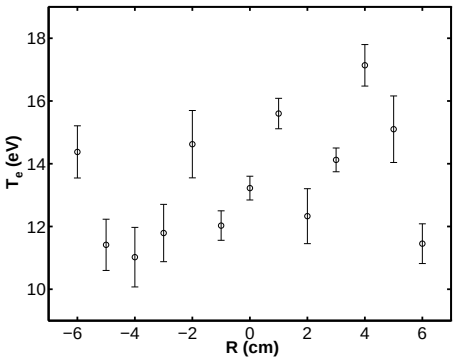

Figure 11. Radial variation of plasma temperature.

(d) *Time evolution of plasma parameters*: The time evolution of plasma density at the centre of the experimental system is shown in figure 12. As can be seen from the figure, initially the density rises but within a few milliseconds stabilizes at about 1.2×10^{10} cm^{-3} and lasts till the microwave power is on (typically a few hundreds of ms).

The time evolution of plasma temperature is also shown in figure 12. As evident from the figure, in the initial part of the discharge, the plasma temperature increases with time and then attains a saturated value ≈50 eV afterwards. This indicates the upper limit of the plasma temperature which can be achieved in such experimental systems.

4.2 *Resonances and cut-offs in the system*

The magnetic field configuration in the system is such that the first two harmonics of ECR reside in the system at $R = 0$ cm (system centre) and $R = 5.5$ cm. The upper hybrid resonance lies at two places because of the symmetric magnetic field in the system at $R = 2$ cm towards the microwave source and at $R = -2$ cm towards the other side of the microwave source as shown in figure 13.

Two cut-offs reside in the plasma system – right-hand X-mode cut-off reside at $R = 5$ cm towards the microwave source and the left-hand X-mode cut-off lies at $R = -5$ cm on the opposite side as shown in figure 14.

4.3 *Power mode conversion coefficient*

Density scale length L_{n} in the system is estimated to be 9.12 cm and magnetic field scale length L_{B} is estimated to be 16.58 cm (from the radial variation of magnetic field). This gives the power mode conversion coefficient C in the system to be 0.85 indicating an appreciable absorption of launched EM waves in the plasma.

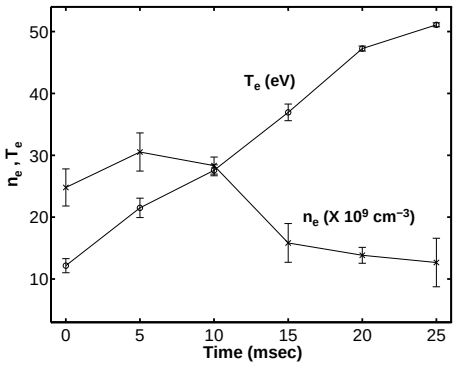

Figure 12. Time evolution of plasma density and plasma temperature.

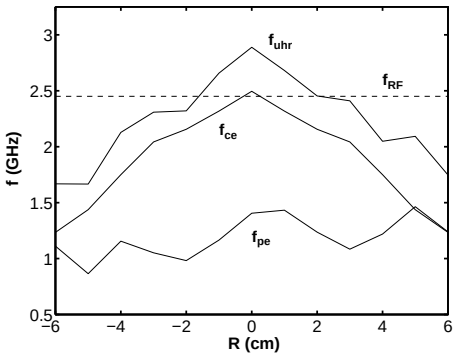

Figure 13. Radial variation of $f_{\rm ce}$, $f_{\rm pe}$ and $f_{\rm uhr}$.

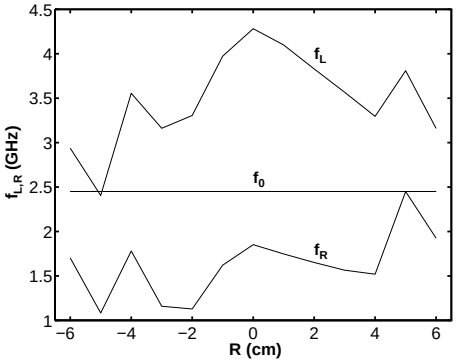

Figure 14. Radial variation of $\omega_{\rm L}$ and $\omega_{\rm R}$.

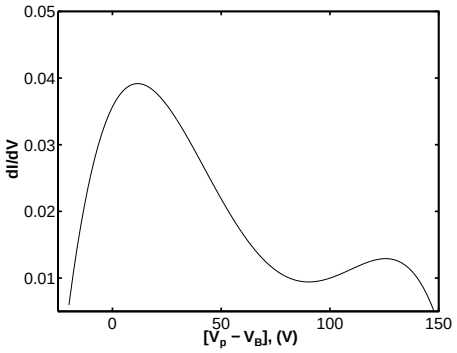

Figure 15. EEDF at the centre of the system.

4.4 *Electron energy distribution function (EEDF)*

The EEDF thus obtained from the Langmuir probe characteristics at the centre of the plasma chamber is shown in figure 15. Here, $(V_{\rm p}-V_{\rm B})$ is the accelerating voltage for the electrons in the plasma and $\mathrm{d}I/\mathrm{d}V$ signifies the number of such electrons. In the figure, the bump in the tail of the distribution indicates the presence of energetic electrons with energies more than 100 eV.

4.5 *Wave electric field measurement*

(a) The wave electric field in the waveguide for an input power of 800 W is E_0 = 6.336 kV/m. Our estimation shows that half of this power is coupled to plasma. The wave electric field then becomes $E_0 = 4.48$ kV/m.

(b) The electric field of the outcoming wave is measured using a dipole probe described in the experimental set-up. The experimentally observed viewing

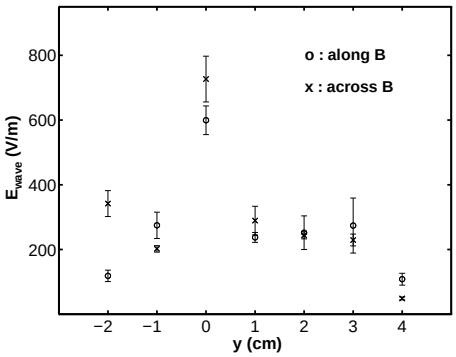

Figure 16. Electric field of the outcoming EM wave.

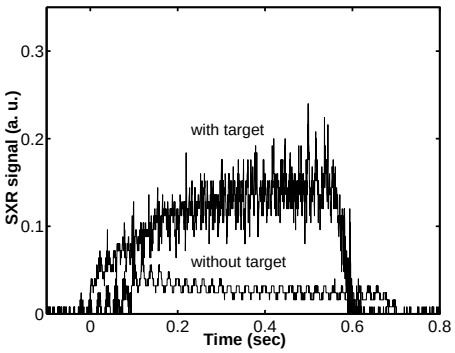

Figure 17. Soft x-ray signal with and without a metal target in plasma.

angle, (ϕ) comes out to be 53.46° (at $y = 0$) which matches well with the theoretically estimated value of 46.8°, discussed in §2. The electric field of the outcoming wave is maximum at this angle as shown in figure 16. In the figure, y denotes the vertical position.

From the calculations above and from the experimental observations, the wave electric field of the outcoming wave is approximately five times less than the estimated wave electric field which indicates the absorption of the launched electromagnetic wave in the plasma and heating it.

4.6 *Ultra-soft x-ray emission*

The ultra-soft x-ray emission from the ECR plasma is observed using a vacuum photodiode (VPD). The soft x-ray emission indicates the presence of heated electrons in the plasma. The complete experiment is described elsewhere [30].

The soft x-ray emission signal with and without any target inside the plasma at an operating pressure of 1×10^{-3} mbar and 800 W launched microwave power is shown in figure 17. The signal without metal target is feeble as compared to the one with Langmuir probe tip made of thoriated tungsten as can be seen in the figure.

Analysing the soft x-ray signals coming out from a metal target hit by energetic electrons is a useful diagnostics [31]. The soft x-ray signal received in the absence of a metal target in the plasma is due to the interaction of energetic electrons with the vessel walls. The presence of a metal target leads to the rapid absorption of the energetic electrons enhancing the soft x-ray flux.

5. Conclusion

Hydrogen plasma is formed in a cylindrical vessel using ECR method with a peak plasma density of 3.2×10^{10} cm^{-3} at first ECR surface and 2.7×10^{10} cm^{-3} at the

second ECR surface at a working pressure of 10^{-3} mbar and with an incident power of ≈800 W. The plasma temperature in the system is between 9 and 15 eV and typical plasma potential is 50 V. ECR heating is observed in the plasma system.

The various cut-offs and resonance locations in the system are identified using the plasma density and plasma temperature radial profiles. The EEDF derived from the Langmuir probe characteristics at the centre of the system shows the presence of energetic electrons in the system.

The power mode conversion coefficient C in the system is estimated to be 0.85 indicating an appreciable absorption of launched EM waves in the plasma system. The absorption of the launched EM waves in the plasma is also confirmed by the reduced wave electric field of the wave coming out of the plasma. The presence of energetic electrons in the plasma is further verified by observing the ultra-soft x-ray emission from the ECR plasma system. The x-ray emission from the system gets enhanced in the presence of a metal (tungsten) target.

The plasma heating in the ECR system could be due to the electrostatic electron Bernstein waves which gets generated at the UHR layer and are absorbed at the ECR surfaces. This can be verified by performing experiments for the obervation of these EBWs and the associated physical phenomena. As a signature of mode conversion, the parametric decay spectrum at the UHR is being investigated experimentally.

Acknowledgement

The authors sincerely acknowledge the referee for his valuable comments which helped in improving the overall outlook of the paper. Also, the authors would like to thank the RF group members at the institute for their kind help at various stages of the experiment.

References

[1] K Rypdal, A Fredriksen, O M Olsen and K G Hellblom, *Phys. Plasmas* **4**, 1468 (1997)
[2] O C Eldridge and A C England, *Nucl. Fusion* **29**, 1583 (1989)
[3] Wallace M Manheimer, Infrared and millimeter waves, in *Instrumentation* (Academic Press, New York, 1979) vol. 2, p. 299
[4] A C England, *IEEE Trans. Plasma Sci.* **PS-12**, 124 (1984)
[5] M Porkolab, L Friedland and I B Bernstein, *Nucl. Fusion* **21**, 1643 (1981)
[6] U Gasparino, *Proc. Eighth Joint Workshop ECE and ECRH*, IPP III/186, **2**, 19 (1993)
[7] D Bora, *Phys. Lett.* **A139**, 308 (1989)
[8] P K Sharma, J P Singh and D Bora, *Plasma Phys. Control. Fusion* **39**, 1669 (1997)
[9] O A Popov, *J. Vac. Sci. Technol.* **A7**, 894 (1989)
[10] O A Popov, *J. Vac. Sci. Technol.* **A8**, 2909 (1990)
[11] A Ganguli, M K Akhtar, R D Tarey and R K Jarwal, *Phys. Lett.* **A250**, 137 (1998)
[12] K S Golovanivsky, *Phys. Rev.* **E52**, 2969 (1995)
[13] H Potts and J Hugill, *Plasma Sources Sci. Technol.* **9**, 18 (2000)
[14] A Ganguli, M K Akhtar and R D Tarey, *Plasma Sources Sci. Technol.* **8**, 519 (1999)

[15] T H Stix, *Waves in plasmas* (American Institute of Physics, New York, 1992) p. 31
[16] D G Swanson, *Theory of mode conversion and tunneling in inhomogeneous plasmas* (John Wiley and Sons, Inc., New York, 1998) p. 27
[17] Francis F Chen, Introduction to plasma physics and controlled fusion, in *Plasma Physics* (Plenum Press, New York, 1984) vol. 127
[18] K G Budden, *The propagation of radio waves* (Cambridge University Press, London, 1985) p. 596
[19] A K Ram and S D Schultz, *Phys. Plasmas* **7**, 4084 (2000)
[20] Noah Hershkowitz, O Auciello and D L Flamm, *Plasma diagnostics: Discharge parameters and chemistry* (Academic Press Inc., San Diego, USA, 1989) vol. 1, p. 113
[21] Von M J Druyvesteyn, *Z. Phys.* **64**, 781 (1930)
[22] V A Godyak, R B Piejak and B M Alexandrovich, *Plasma Sources Sci. Technol.* **1**, 36 (1992)
[23] T Lagarde, Y Arnal, A Lacoste and J Pelletier, *Plasma Sources Sci. Technol.* **10**, 181 (2001)
[24] Samuel Y Liao, *Microwave devices and circuits* (Prentice-Hall of India Pvt. Ltd, New Delhi, 2000) p. 116
[25] H P Laqua, V Erckmann, H J Hartfuß and H Laqua, W7-AS Team and ECRH Group, *Phys. Rev. Lett.* **78**, 3467 (1997)
[26] H P Laqua, H J Hartfuß and W7-AS Team, *Phys. Rev. Lett.* **81**, 2060 (1998)
[27] I Langmuir, *Phys. Rev.* **36**, 954 (1929)
[28] Ashwani Kumar and R Bhaskaran, *Rev. Sci. Instrum.* **63**, 4439 (1992)
[29] R Bhaskaran and T Selvakumaran, *Rev. Sci. Instrum.* **70**, 2637 (1999)
[30] Vipin K Yadav and D Bora, *Plasma Sources Sci. Technol.* **13**, 231 (2004)
[31] I H Hutchinson and A H Morton, *Nucl. Fusion* **16**, 447 (1976)